Applied Mathematical Modelling 39 (2015) 2951–2961

Contents lists available at ScienceDirect

Applied Mathematical Modelling

journal homepage: www.elsevier.com/locate/apm

Nonlinear dynamic analysis of a single-machine infinite-bus power system

Xiaodong Wang [a,*], Yushu Chen [a], Gang Han [a], Caiqin Song [b]

[a] School of Astronautics, Harbin Institute of Technology, PO Box 137, Harbin 150001, China
[b] School of Mathematical Sciences, University of Jinan, Jinan 250022, China

ARTICLE INFO

Article history:
Received 13 September 2012
Received in revised form 23 September 2014
Accepted 7 November 2014
Available online 26 November 2014

Keywords:
SMIB power system
Swing equation
Chaotic motion
Melnikov's method

ABSTRACT

This study focuses on the nonlinear dynamic characteristics of a single-machine infinite-bus (SMIB) power system under a periodic load disturbance. The qualitative behavior of this system is described by the well-known "swing equation", which is a nonlinear second-order differential equation. Compared with the existing results, the generator damping in this paper, which is more close to the practical engineering, is related to the state variables of this system. In addition, Melnikov's method is applied to obtain the threshold for the onset of chaos. The efficiency of the criteria for chaotic motion is verified via numerical simulations. Comparisons between the theoretical analysis and numerical simulation show good agreements. The results in this paper will contribute a better understanding of the nonlinear dynamic behaviors of the SMIB power system.

1. Introduction

Power system instability is one of the main reasons for large-scale blackouts all over the world in the past twenty years. Modern power system is forced to operate close to its stability limit due to the growth of power demand and other constraints for building new power plants and transmission lines, such as environment, technique and economic. Recently, electric power systems have become more huge and complicated. Stability problems have become more complex as interconnections become more extensive [1]. Therefore, the stability of electric power systems has been received much attention in scientific studies [2–5].

In the field of power system, many researchers paid close attention to the dynamic characteristics related to the power system stability, especially on an equivalent single-machine infinite-bus (SMIB) power system. Duan et al. [6] investigated the bifurcations associated with sub-synchronous resonance of a SMIB power system with series of capacitor compensation. They pointed out that torus bifurcation and periodical fold bifurcation may occur in this system. Zhu and Mohler [7] gave a Hopf bifurcation analysis for a SMIB power system with sub-synchronous resonance (SSR) by applying Hopf bifurcation theorem. Wei et al. [8,9] examined the influences of Gaussian white noise on the dynamic behaviors of a fundamental power system model. Chen et al. [10] studied the chaotic control and chaotification problem of a SMIB power system, where the power of the machine was assumed to be a simple harmonic quantity. Moreover, the Melnikov's method works effectively for discussing bifurcations of periodic orbits and homo-(hetero-)clinic orbits for dynamical systems. For instance, this method has been applied in a classical SMIB power system model [11–13]. The condition is given under which the

* Corresponding author. Tel.: +86 451 86402822.
E-mail addresses: wangxdhit@gmail.com (X. Wang), yschen@hit.edu.cn (Y. Chen).

http://dx.doi.org/10.1016/j.apm.2014.11.018
0307-904X/

Nomenclature

δ	rotor angle
ω	rotor angular speed
ω_R	synchronous angular speed
$\Delta\omega$	angular speed deviation
H	inertia constant of the synchronous machine
P_E	electrical power output of the synchronous machine
P_M	mechanical power input to the synchronous machine
E	voltage magnitude of the machine
X	total reactance of the system
D	damping coefficient
Ω	disturbance frequency
P_D	disturbance amplitude
x'_d	transient reactance of the machine
x_T	reactance of the transformer
U	voltage of the infinite busbar

heteroclinic orbit persists with small perturbations. Chaotic and sub-harmonic oscillations of the SMIB power system were discussed in [14] by computing Melnikov functions with the residue of a complex function and elliptic integrals. Nayfeh et al. [15,16] investigated the period-doubling bifurcations, the chaotic motion, and the loss of synchronism in a single-machine quasi-infinite busbar system. In their studies, the method of multiple scales was used to develop an approximate first order closed-form expression for the period-one response. Abed and Varalya [17] showed that the classical swing equation for a power generator might undergo a Hopf bifurcation to periodic solutions if this system was augmented to include a changeable net damping, which was in reality a function of the state of the system.

To the best of our knowledge, the damping of the synchronous generator is regarded as a constant in those previous studies [8–12,14–16]. However, the damping power of the synchronous generator in the actual power system is not a constant but a function related to the state variables of the system. It depends on the rotor angle δ and fluctuates with the rotor speed deviation $\Delta\omega = \mathrm{d}\delta/\mathrm{dt}$. For small speed deviations the damping power is proportional to speed deviation, while for larger speed deviations it is a nonlinear function of speed deviation. If the damping is taken as a constant, it cannot exactly reflect the nonlinear dynamic characteristics of the system. In fact, when the well-known Melnikov's method is used to obtain the criteria for the occurrence of chaotic motion, the mathematical expressions of the homoclinic orbits need to be calculated. It is worth noting that the analytical expression of the homoclinic orbits in the SMIB power system is difficult to obtain. Therefore, the mechanical power input to the synchronous generator is considered as a small quantity or zero in the existing literature. In this case, the original homoclinic orbits have changed into heteroclinic orbits, so the intrinsic characteristic of this system is also changed. Based on the two major problems mentioned above, the purpose of this paper is to study the rotor angle stability of a more accurate SMIB system. The work in this paper differs from the existing literature in two aspects, one is the damping of the synchronous generator, and the other is the application of the Melnikov's method.

The remainder of this paper is organized as follows. Section 2 introduces the modified equation of the SMIB power system with nonlinear damping. In Section 3, the Melnikov's method is applied to obtain the criteria for chaotic motion occurrence in this system. In Section 4, numerical simulations are carried out to show the nonlinear dynamic behaviors of this system. Concluding remarks are given in Section 5.

2. The mathematical model of a SMIB power system

The configuration of the single-machine infinite-bus (SMIB) power system in this study is shown in Fig. 1, where the synchronous generator S_1 is delivering power to the infinite-bus through a transmission line. 3 and 4 are the equivalent main transformer of system 1 and 2, respectively. 5, 6 and 7 are load, circuit breaker, and systematic tie line, respectively. The swing equation [1] describing the angle dynamics of the synchronous generator in Fig. 1 can be written as

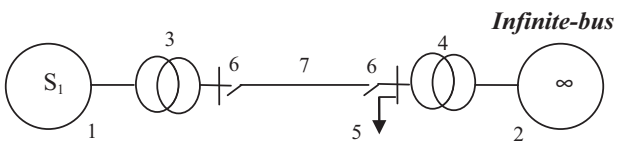

Fig. 1. Single-machine infinite-bus (SMIB) power system model.

$$\begin{cases} \frac{d\delta}{dt} = \Delta\omega = \omega - \omega_R, \\ \frac{2H}{\omega_R}\frac{d\Delta\omega}{dt} = P_M - P_E, \end{cases} \tag{1}$$

where δ is the rotor angle measured with respect to a synchronously rotating reference frame moving with constant angular velocity ω_R, ω is angular speed, $\Delta\omega$ is angular speed deviation. H is the inertia constant of the machine, P_E, P_M are electrical power and mechanical power, respectively.

When the generator is a non-salient pole generator and the transmission line is non-loss, the electrical power P_E is

$$P_E = \frac{UE}{X}\sin\delta = P_s \sin\delta,$$

where $U\angle 0^0$ is the reference phasor of the infinite busbar, E is the voltage of the machine, X is the total reactance of the system.

Supposing system (1) is subjected to a periodic load disturbance with the amplitude P_D and frequency Ω, consider the damping of synchronous generator, system (1) can be rewritten as

$$\begin{cases} \frac{d\delta}{dt} = \Delta\omega, \\ \frac{2H}{\omega_R}\frac{d\Delta\omega}{dt} = P_M - P_S\sin\delta - D\Delta\omega + P_D\cos(\Omega t), \end{cases} \tag{2}$$

where D is the damping coefficient. In order to simplify the analysis, the following transforms are introduced:

$$\tau = t\sqrt{\frac{\omega_R P_S}{2H}}, \quad x(\tau) = \delta(t), \quad y(\tau) = \sqrt{\frac{2H}{\omega_R P_S}}\Delta\omega(t), \quad c = D\sqrt{\frac{\omega_R}{2HP_S}}, \quad 0 < \rho = \frac{P_M}{P_S} \leqslant 1, \quad f = \frac{P_D}{P_S}, \quad \bar{\omega} = \Omega\sqrt{\frac{2H}{\omega_R P_S}}, \tag{3}$$

then the system (1) becomes

$$\begin{cases} \frac{dx}{d\tau} = y, \\ \frac{dy}{d\tau} = -\sin x - cy + \rho + f\cos(\bar{\omega}\tau). \end{cases} \tag{4}$$

In order to understand the fundamental behavior of the SMIB system, a case with no damping and no external excitation is considered firstly. For $c = 0, f = 0$, Eq. (4) takes the form

$$\begin{cases} \frac{dx}{d\tau} = y, \\ \frac{dy}{d\tau} = -\sin x + \rho. \end{cases} \tag{5}$$

The equilibriums of system (5) can be represented as

$$E : (x_1, 0) = (\arcsin\rho, 0), \quad P_0 : (x_2, 0) = (\pi - \arcsin\rho, 0).$$

The Jacobian matrix of equilibrium $(x_1, 0)$ is given by

$$J = \begin{pmatrix} 0 & 1 \\ -\sqrt{1-\rho^2} & 0 \end{pmatrix},$$

with the characteristic equation written as

$$\lambda^2 + \sqrt{1-\rho^2} = 0,$$

and the eigenvalues are $\lambda_{1,2} = \pm i\sqrt{1-\rho^2}$. So the equilibrium $(x_1, 0)$ is a center.

The Jacobian matrix of equilibrium $(x_2, 0)$ is obtained as

$$J = \begin{pmatrix} 0 & 1 \\ \sqrt{1-\rho^2} & 0 \end{pmatrix},$$

with eigenvalues $\lambda_{1,2} = \pm\sqrt{1-\rho^2}$. Thus the equilibrium $(x_2, 0)$ is a saddle point.

Fig. 2 shows the phase portraits (trajectories) of system (5) for different initial conditions. The phase trajectory in the form of circle 1 is oscillating orbit. The angular displacement is always smaller and the angular velocity changes its sign twice per period. Trajectory 3 depicts a typical rotational motion. The angular displacement is growing with time. Trajectory 2 is a homoclinic orbit in which the unstable manifold merges with the stable manifold at the saddle point P_0. It is necessary to pass through the homoclinic orbit in order to travel from oscillatory to rotational motion, and this means that a homoclinic bifurcation (global bifurcation) occurs.

To examine the influence of the parameter ρ on the dynamic characteristic of system (5), we construct the diagram (Fig. 3a) which describes the position of the two equilibrium points as the parameter ρ varies. The upper dashed branch marks the position of the saddle point, while the lower solid branch marks the position of the center point. Our observation is that these two equilibrium points get close to each other with the increase of the parameter ρ and overlap together at a critical point, especially when $\rho = 1$ (as shown in Fig. 3b). This point is a center-saddle bifurcation point corresponding to the stable and unstable critical running point of the synchronous generator, the system is in a static stability limit state.

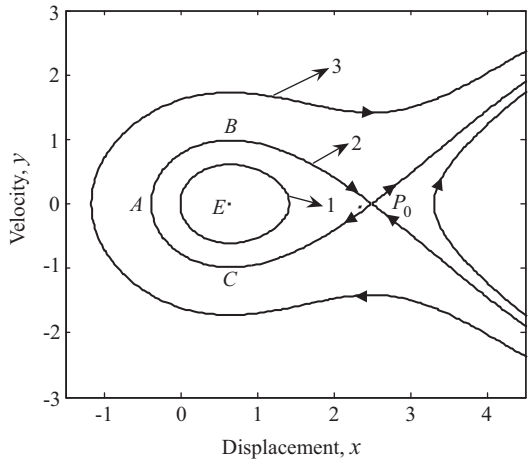

Fig. 2. Phase trajectories for the unperturbed system (5).

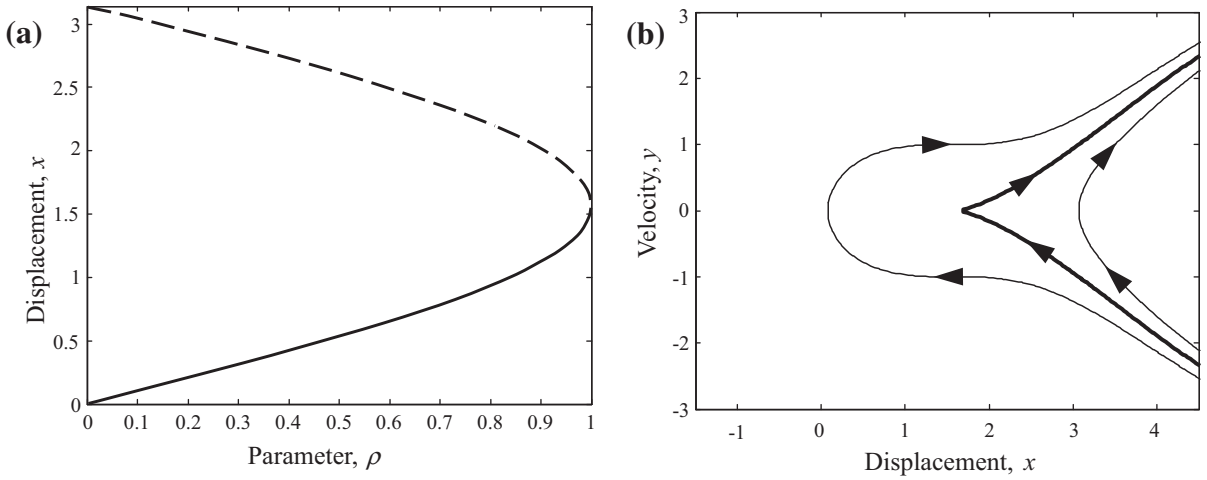

Fig. 3. (a) Equilibrium bifurcation diagram of unperturbed system (5); (b) phase trajectories of unperturbed system (5) for $\rho = 1$.

The modification is made in Eq. (4) by taking a van der Pol damping. Define $c = \xi + \gamma x^2$, where ξ and γ take constant values according to the actual operating conditions. Obviously, the damping coefficient is comprised of two parts: the constant term and the nonlinear term. The latter is proportional to the quadratic term of the state variable. It is closer to the real power system according to the modified damping model [18]. Therefore, we can obtain the following equation

$$\begin{cases} \frac{dx}{d\tau} = y, \\ \frac{dy}{d\tau} = -\sin x - (\xi + \gamma x^2)y + \rho + f\cos(\bar{\omega}\tau). \end{cases} \tag{6}$$

3. Melnikov analysis

In this section, we focus our attention on the existence of chaos in Eq. (6). Melnikov's method is a powerful approximate tool for investigating chaos occurrence in near Hamiltonian systems, and has been successfully applied to the analysis of chaos in smooth systems. To our knowledge, the existence of a simple zero of the Melnikov function implies the possible occurrence of chaos in the sense of Smale horseshoes, for details please see [19].

In order to apply the Melnikov's method to study the transversality condition, we rewrite the SMIB system (6) as

$$\begin{cases} \frac{dx}{d\tau} = y, \\ \frac{dy}{d\tau} = -\sin x + \rho + \varepsilon[-(\xi + \gamma x^2)y + f\cos(\bar{\omega}\tau)]. \end{cases} \tag{7}$$

If $\varepsilon = 0$, the following Hamiltonian function of Eq. (6) can be obtained

$$H(x,y) = \frac{1}{2}y^2 - \cos x - \rho x + H_0, \tag{8}$$

where H_0 is a integral constant.

By using the Hamiltonian function (8), the phase portrait is plotted as shown in Fig. 2. Let $H(x_E, y_E) = 0$, it stands for the homoclinic orbit of the unperturbed system passing through the center point $(x_1, 0) = (\arcsin\rho, 0)$, then it yields to

$$H_0 = \arcsin\rho + \cos(\arcsin\rho).$$

Hence the homoclinic orbit P_0CABP_0 in Fig. 2 satisfies

$$\frac{1}{2}y^2 - \cos x - \rho x = \cos(\arcsin\rho) - \rho\pi + \rho\arcsin\rho \hat{=} H(\rho). \tag{9}$$

Supposing the homoclinic orbit can be expressed by the parametric function $[x(\tau), y(\tau)]$, we have

$$\lim_{\tau\to\pm\infty}[x(\tau), y(\tau)] = P_0,$$

$$y(\tau) = \pm\sqrt{2H(\rho) + 2\cos x(\tau) + 2\rho x(\tau)}. \tag{10}$$

(a) The coordinate of point A in Fig. 2 is $[x(0), y(0)]$, where $y(0) = 0$ and $x(0)$ satisfies the equation $\rho x(0) + \cos(x(0)) - \rho\pi + \rho\arcsin\rho + \cos(\arcsin\rho) = 0$.

(b) If $\tau \in (-\infty, 0]$, $[x(\tau), y(\tau)]$ represents the lower part of the homoclinic orbit, which is marked as P_0CA. On the contrary, when $\tau \in [0, \infty)$, $[x(\tau), y(\tau)]$ stands for the upper part of the homoclinic orbit marked as ABP_0. Here $x(\tau)$ is an even function and $y(\tau)$ is an odd function.

Next, we introduce the following notation in system (7)

$$y = \dot{x}, \quad X = \begin{pmatrix} x \\ y \end{pmatrix}, \quad f(X) = \begin{pmatrix} y \\ -\sin(x) + \rho \end{pmatrix}, \quad g(X) = \begin{pmatrix} 0 \\ -(\xi + \gamma x^2)y + f\cos\bar{\omega}\tau \end{pmatrix}.$$

For the homoclinic orbit, we get

$$tr(Df) = \begin{pmatrix} 0 & 1 \\ -\cos(x) & 0 \end{pmatrix} = 0,$$

and

$$f(X(\tau)) \wedge g(X(\tau), \tau + \tau_0) = [-(\xi + \gamma x^2(\tau))y^2(\tau) + y(\tau)f\cos\bar{\omega}(\tau + \tau_0)],$$

where the operator $\wedge$ is defined as

$$a \wedge b = a_1 b_2 - a_2 b_1,$$

for any $a = (a_1, a_2)^T$ and $b = (b_1, b_2)^T$.

The corresponding Melnikov function of Eq. (7) is given by

$$\begin{aligned} M(\tau_0) &= \int_{-\infty}^{\infty}[f(X(\tau)) \wedge g(X(\tau), \tau + \tau_0)]e^{-\int_0^\tau tr(Df(X(z)))dz}dt = \int_{-\infty}^{\infty}[-(\xi + \gamma x^2(\tau))y^2(\tau) + y(\tau)f\cos\bar{\omega}(\tau + \tau_0)]dt \\ &= -\xi\int_{-\infty}^{+\infty} y^2(\tau)d\tau - \gamma\int_{-\infty}^{\infty} x^2(\tau)y^2(\tau)d\tau + f\int_{-\infty}^{+\infty} y(\tau)\cos\bar{\omega}(\tau + \tau_0)]d\tau = -\xi\bar{A} - \gamma\bar{B} + f\bar{C}, \end{aligned}$$

where

$$\bar{A} = \int_{-\infty}^{+\infty} y^2(\tau)d\tau, \quad \bar{B} = \int_{-\infty}^{\infty} x^2(\tau)y^2(\tau)d\tau, \quad \bar{C} = \int_{-\infty}^{+\infty} y(\tau)\cos\bar{\omega}(\tau + \tau_0)]d\tau.$$

By calculation, we can obtain the following equations

$$\bar{A} = \int_{-\infty}^{+\infty} y^2(\tau)d\tau = 2\int_0^{+\infty} y^2(\tau)d\tau = 2\int_{x_A}^{x_{P_0}} y(\tau)dx = 2\int_{x_A}^{x_{P_0}} \sqrt{2H(\rho) + 2\cos x + 2\rho x}dx \tag{11}$$

and

$$\bar{B} = \int_{-\infty}^{\infty} x^2(\tau)y^2(\tau)d\tau = 2\int_0^{\infty} x^2(\tau)y^2(\tau)d\tau = 2\int_{x_A}^{x_{P_0}} x^2(\tau)y(\tau)dx = 2\int_{x_A}^{x_{P_0}} x^2\sqrt{2H(\rho) + 2\cos x + 2\rho x}dx. \tag{12}$$

From Eq. (10), it follows that

$$\frac{dx}{d\tau} = \pm\sqrt{2H(\rho) + 2\cos x(\tau) + 2\rho x(\tau)}.$$

It turns out that

$$\pm d\tau = \frac{dx}{\sqrt{2H(\rho) + 2\cos x + 2\rho x}}.$$

Integrating both sides, it follows that

$$\pm\tau = \int_{x_A}^{x} \frac{dx}{\sqrt{2H(\rho) + 2\cos x + 2\rho x}}.$$

The integral $\bar{C}$ is

$$\begin{aligned}\bar{C} &= \int_{-\infty}^{+\infty} y(\tau)\cos\bar{\omega}(\tau+\tau_0)]d\tau = \int_{-\infty}^{+\infty} y(\tau)\cos\bar{\omega}\tau_0\cos\bar{\omega}\tau d\tau - \int_{-\infty}^{+\infty} y(\tau)\sin\bar{\omega}\tau_0\sin\bar{\omega}\tau d\tau \\ &= -2\sin\bar{\omega}\tau_0\int_0^{+\infty} y(\tau)\sin\bar{\omega}\tau d\tau = -2\sin\bar{\omega}\tau_0\int_{x_A}^{x_{P_0}} \sin\bar{\omega}\tau dx \\ &= -2\sin\bar{\omega}\tau_0\int_{x_A}^{x_{P_0}} \sin\bar{\omega}\left[\pm\int_{x_A}^{x}\frac{d\theta}{\sqrt{2H(\rho)+2\cos\theta+2\rho\theta}}\right]dx. \end{aligned} \tag{13}$$

In the Eqs. (11)–(13), x_A and x_{P_0} are the horizontal ordinates of the points A and P_0 respectively, where the homoclinic orbit in Fig. 2 intersects the x axis.

It can be seen that

$$M(\tau_0) = -\xi\bar{A} - \gamma\bar{B} - \sin\bar{\omega}\tau_0 f\bar{C} = 0,$$

has a simple zero root for τ_0 if and only if the following inequality holds

$$|f| \geqslant \left|\frac{\xi\bar{A} + \gamma\bar{B}}{\bar{C}}\right|.$$

The Melnikovian detected chaotic boundary of Eq. (6) is obtained, as shown in Fig. 4 for different values of parameters $\rho = 0.5, 0.6$. In the area above the detected boundaries, chaotic motions will be generated, i.e. in the area of $|f| \geqslant (\xi\bar{A} + \gamma\bar{B})/\bar{C}$. Furthermore, in order to verify the criterion obtained in this section, a numerical simulation has been carried out by fixing parameters $\rho = 0.50, \xi = 0.35, \gamma = 0.02, \bar{\omega} = 1.0$. A bifurcation diagram by examining a graph of the velocity y versus the external excitation amplitude f is given in Fig. 5, from which periodic windows and chaotic regions can be clearly seen as parameter f changes. Note that the chaotic criterion detected by using Melnikov's method is 0.7256, while it is 0.7259 in the numerical simulation. Comparisons between them show good agreements.

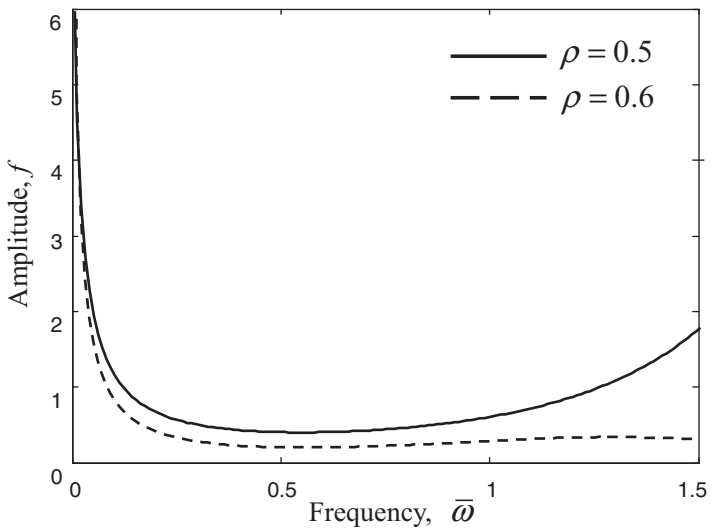

Fig. 4. Chaotic boundaries for system (6) detected by using the Melnikov's method.

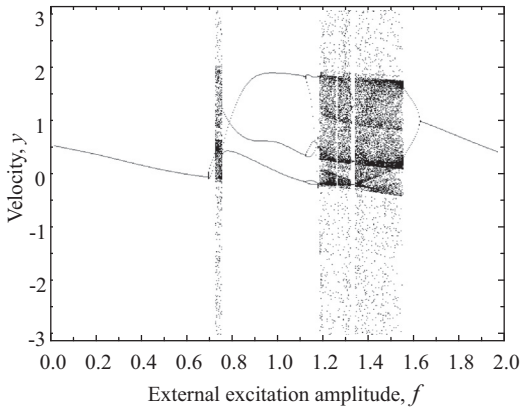

Fig. 5. Bifurcation diagram for velocity y versus the external excitation amplitude f.

4. Numerical simulations

In this section, numerical simulations have been carried out to verify the results of the theoretical analysis and to better understand the changes of the dynamic characteristic for the SMIB power system as the periodic load and the damping vary. Numerical studies have been carried out using *Dynamics* [20] which allows one to investigate the complicated dynamic behaviors of the SMIB power system by considering bifurcation diagrams, Lyapunov exponents, Poincaré maps, and phase trajectories. The time histories are plotted by using the fourth-order Runge–Kutta method with the software *Matlab*. As an illustrative example, consider a specific system with the system parameters, they are Rated MVA = 160, Rated PF = 0.85, Rated kV = 15, $\omega_R = 120\pi$, $x'_d = 0.35$. The rest parameters of the SMIB power system are $H = 0.5, P_M = 0.5$, $D_1 = 0.35, D_2 = 0.02, U = 1, x_T = 0.65, X = x'_d + x_T = 1$ (converted to per unit). D_1 and D_2 refer to the constant and nonlinear damping coefficient, respectively. A parameter as a bifurcation parameter is selected, and the other system parameters are fixed. Bifurcation diagrams are plotted to investigate the effects of varying the selected system parameter for typical ranges.

4.1. Effect of the external excitation

For the SMIB power system, we select the excitation amplitude f as the bifurcation parameter to construct the bifurcation diagram (as shown in Fig. 5) for specific parameters $\rho = 0.50$, $\xi = 0.35$, $\gamma = 0.02$, $\bar{\omega} = 1.0$. The corresponding largest Lyapunov exponent diagram versus the parameter f is shown in Fig. 6. It is generally known that if the largest value in the spectrum of Lyapunov exponents is positive, then the system is chaotic [21]. According to Fig. 5, it is easy to see that the period doubling bifurcation leads to chaos, which is confirmed by the largest Lyapunov exponent in Fig. 6.

As the excitation amplitude f increases, the rotor angle oscillation changes in terms of the sequence of period-1, period-2 motion and chaotic motion. Fig. 7a and b show the phase portrait and the time history of period-1 motion for $f = 0.60$. Fig. 8a

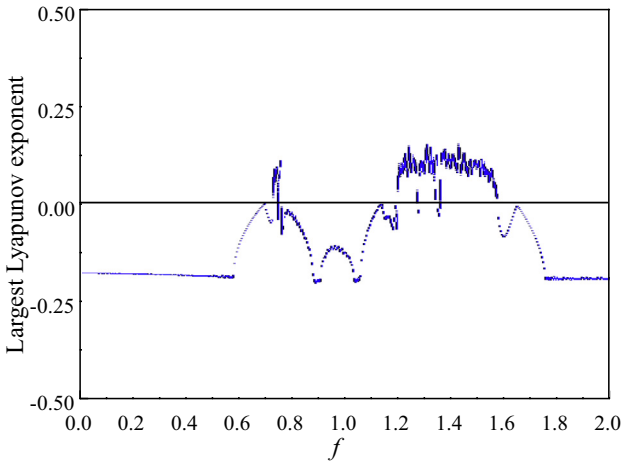

Fig. 6. Largest Lyapunov exponents versus f.

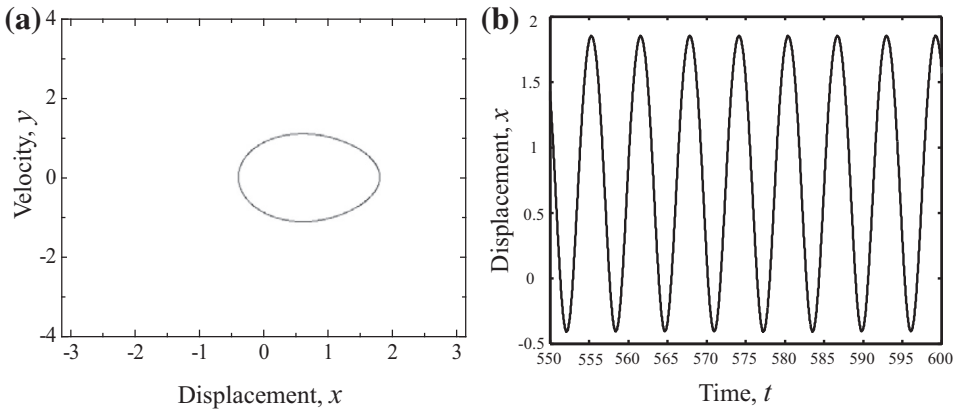

Fig. 7. (a) Phase portrait; (b) time history for $f = 0.60$ (period-1 T).

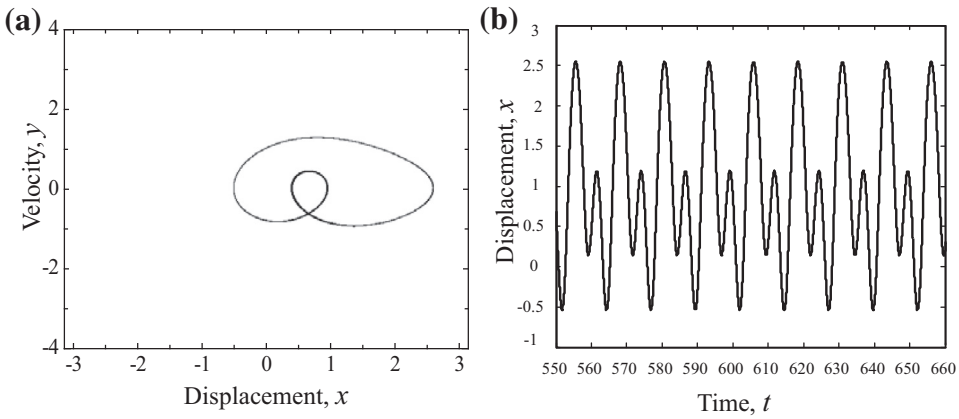

Fig. 8. (a) Phase portrait; (b) time history for $f = 0.72$ (period-2 T).

and Fig. 8b show the phase portrait and the time history of period-2 motion for $f = 0.72$. When $f = 0.7259$, the chaotic motion occurs. The rotor angle shows random-like chaotic oscillation. As can be seen in the bifurcation diagram (Fig. 5), the first chaotic region is very narrow. Fig. 9a and Fig. 9b show the phase portrait of chaotic motion and the chaotic attractor for $f = 0.7259$, respectively. When the excitation amplitude becomes larger, the chaotic attractor breaks up. As shown in Fig. 10, for $f = 0.79$ the rotating motion occurs, which makes the response of the system become unbounded and lose

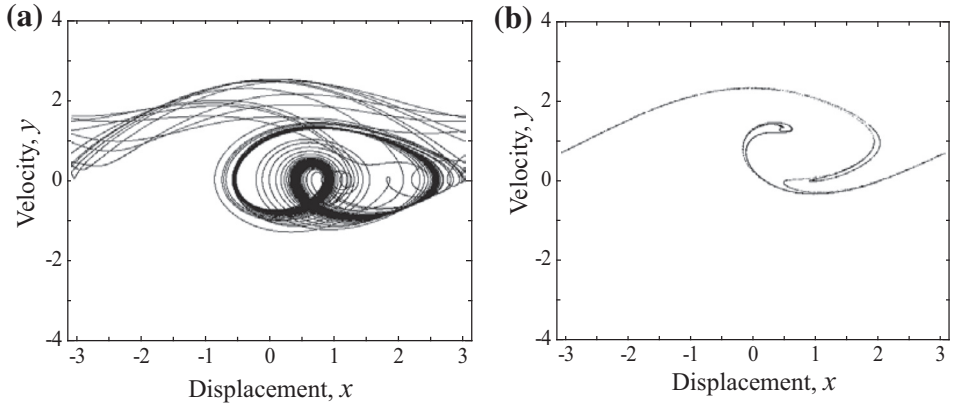

Fig. 9. (a) Phase portrait of chaotic motion; (b) Poincaré map of the chaotic attractor for $f = 0.7259$.

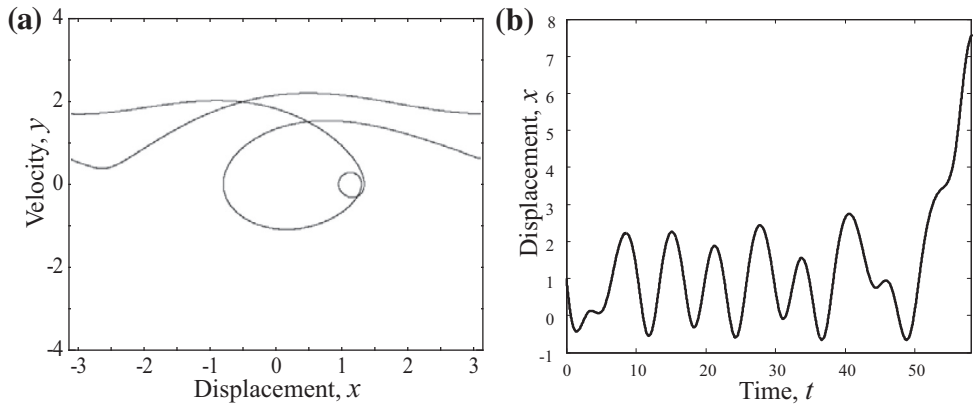

Fig. 10. (a) Phase portrait of the rotating orbits and (b) time history for $f = 0.79$.

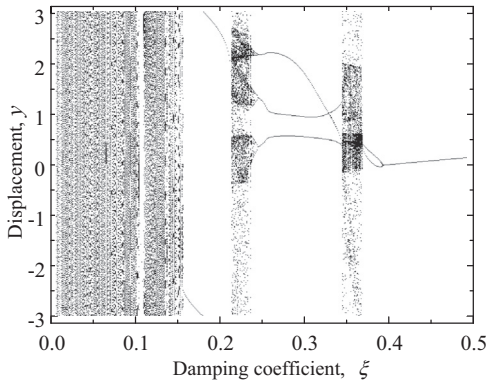

Fig. 11. Bifurcation diagram: y versus ξ for $\rho = 0.50, \gamma = 0.02, f = 0.75, \varpi = 1.0$.

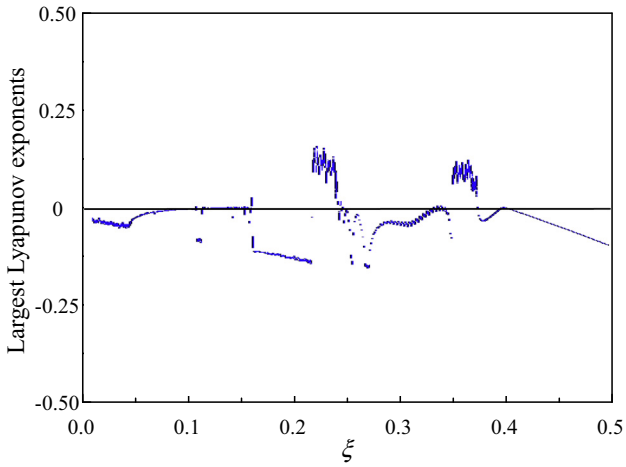

Fig. 12. Largest Lyapunov exponents versus ξ.

synchronism. Moreover, as the power angle δ increases, the electrical power P_E becomes larger, which causes the rotor of the synchronous generator to accelerate. The system eventually loses its stability due to the increase of the oscillation amplitude.

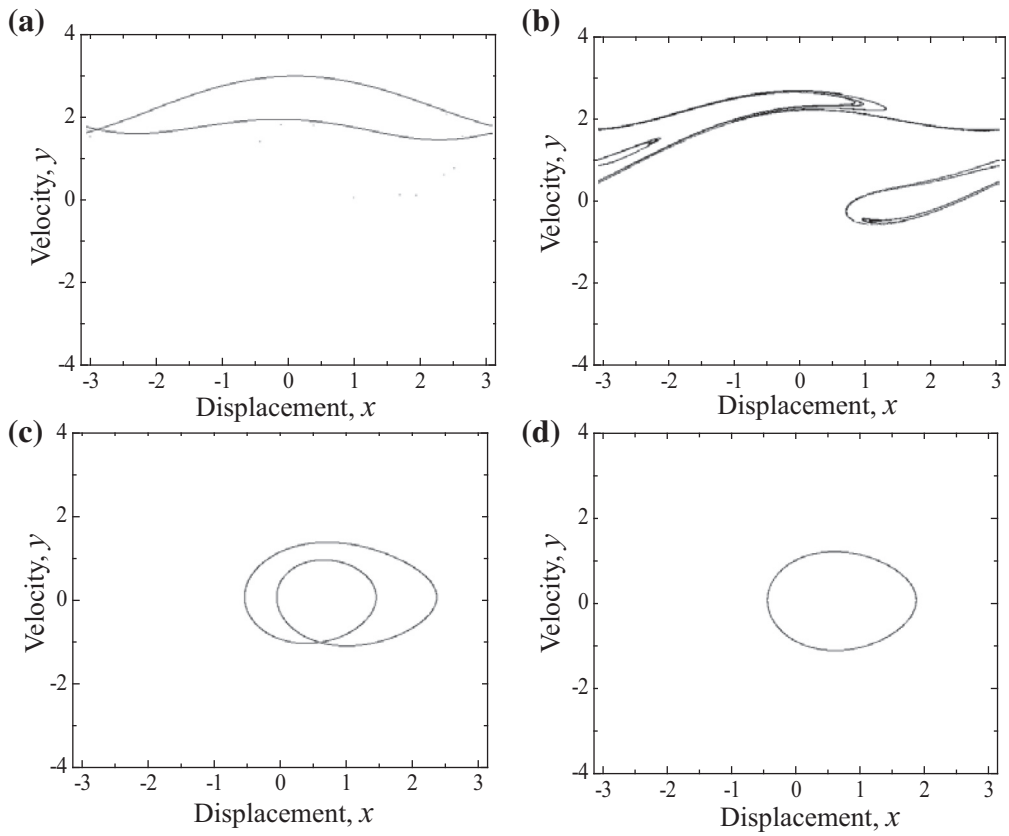

Fig. 13. (a) Phase portrait of the rotating orbits for $\xi = 0.18$; (b) Poincaré map of the chaotic attractor for $\xi = 0.22$; (c) phase portrait for $\xi = 0.38$ (period-2 T); (d) phase portrait for $\xi = 0.45$ (period-1 T).

4.2. Effect of the nonlinear damping

As discussed in the previous subsection, the effect of the nonlinear damping on the dynamic behaviors of the SMIB power system is very critical and is worth studying. Without loss of generality, we choose the constant damping coefficient ξ as the bifurcation parameter. Fig. 11 shows the bifurcation diagram of the system by examining the graph of the velocity y versus the constant damping coefficient ξ, for $\rho = 0.50$, $\gamma = 0.02$, $f = 0.75$, $\bar{\omega} = 1.0$. The corresponding largest Lyapunov exponent diagram versus the parameter ξ is shown in Fig. 12. When ξ is very small, the system exhibits a dynamic response of the chaotic motion. When ξ gradually increases, the system gives a transition from chaotic motion to periodic motion. Specific results are provided in the following figures. Fig. 13a shows the phase portrait of the rotating orbit for $\xi = 0.18$, i.e. the synchronous generator is in loss of synchronism. The chaotic attractor for $\xi = 0.22$ is given in Fig. 13b. The phase portraits of the period-2, period-1 motions for $\xi = 0.38$ and $\xi = 0.45$ are shown in Fig. 13c and in Fig. 13d, respectively.

Our numerical results also demonstrate that the structure damping of the synchronous generator has a significant impact on the stable operation of the SMIB power system when the external perturbation remains unchanged. When the damping is small, out-of-step motion or chaotic motion may occur. By increasing the damping, these movements can be settled down to a periodic motion with small amplitude.

5. Conclusions

In this paper, the dynamics of a fundamental power system model in a single-machine infinite-bus representation is analyzed by using theoretical analysis and numerical simulations. Our results extend the existing literature by considering a more practical damping model of the synchronous generator, which is related to the state variables of the system. The Melnikov's method is successfully applied to obtain the threshold for the onset of chaotic motion. The numerical simulations show that the external excitation and the nonlinear damping have significant influence on the nonlinear dynamic behaviors of this system. Their changes make the system undergo a period-doubling bifurcation. The sequence of period-doubling bifurcation continues until it culminates in a chaotic motion. Beyond the chaotic motion, the loss of synchronism occurs. This

is one way in which the system loses its stability. These conclusions can provide useful guidance for understanding a power system secure operation.

Overall, the results presented in this paper provide a detailed understanding of the nonlinear dynamic response of a SMIB power system under a periodic load disturbance. The nonlinear dynamic analysis of a more detailed large scale power system promises to be an exciting and interesting research subject, which can be pursued in our future research. The Melnikov's method used in this paper also needs to be developed in a large scale power system including more synchronous generators in the future.

Acknowledgements

The authors would like to thank the reviewers and the editors for their constructive comments and suggestions which improved the quality of this paper. The authors acknowledge the financial support of the National Basic Research Program of China (973 Program) with the Grant No. 2015CB057405.

References

[1] Q. Lu, Y.Z. Sun, Nonlinear Control of Power System, China Science Press, Beijing, 1993.
[2] E.P. Gerardo, M.O. Paul, D.C. Arnau, M. Jaime, Output-feed back IDA stabilisation of an SMIB system using a TCSC, Int. J. Control 83 (12) (2010) 2471–2482.
[3] J. Shi, Y. Tang, T. Dai, L. Ren, J. Li, S. Cheng, Determination of SMES capacity to enhance the dynamic stability of power system, Physica C 470 (20) (2010) 1707–1710.
[4] N.S. Manjarekar, R.N. Banavar, R. Ortega, Application of interconnection and damping assignment to the stabilization of a synchronous generator with a controllable series capacitor, Int. J. Electr. Power Energy Syst. 32 (1) (2010) 63–70.
[5] R. Chendur Kumaran, T.G. Venkatesh, K.S. Swarup, Voltage stability – case study of saddle node bifurcation with stochastic load dynamics, Int. J. Electr. Power Energy Syst. 33 (8) (2011) 1384–1388.
[6] X.Z. Duan, J.Y. Wen, S.J. Cheng, Bifurcation analysis for an SMIB power system with series capacitor compensation associated with sub-synchronous resonance, Sci. China Ser. E 52 (2) (2009) 436–441.
[7] W. Zhu, R.R. Mohler, Hopf bifurcations in a SMIB power system with SSR, IEEE Trans. Power Syst. 11 (3) (1996) 1579–1584.
[8] D.Q. Wei, X.S. Luo, Noise-induced chaos in single-machine infinite-bus power systems, Europhys. Lett. 86 (5) (2009).
[9] D.Q. Wei, Bo. Zhang, D.Y. Qiu, X.S. Luo, Effect of noise on erosion of safe basin in power system, Nonlinear Dyn. 61 (2010) 477–482.
[10] H.K. Chen, T.N. Lin, J.H. Chen, Dynamic analysis, controlling chaos and chaotification of a SMIB power system, Chaos Solitons Fractals 24 (2005) 1307–1315.
[11] L.F.C. Alberto, N.G. Bretas, Application of Melnikovs method for computing heteroclinic orbits in a classical SMIB power system model, IEEE Trans. Circuits Syst. I 47 (7) (2000) 1085–1089.
[12] W.N. Zhang, W.D. Zhang, Chaotic oscillation of a nonlinear power system, Appl. Math. Mech. 20 (10) (1999) 1175–1183.
[13] B. Yuan, W.X. Ma, Chaos in the almost periodic forcing electrical power systems, Autom. Electr. Power Syst. 18 (5) (1994) 26–30 (in Chinese).
[14] X.W. Chen, W.N. Zhang, W.D. Zhang, Chaotic and subharmonic oscillations of a nonlinear power system, IEEE Trans. Circuits Syst. II 52 (12) (2005) 811–815.
[15] M.A. Nayfeh, A.M.A. Hamdan, A.H. Nayfeh, Chaos and instability in a power system: subharmonic-resonant case, Nonlinear Dyn. 2 (1991) 53–72.
[16] M.A. Nayfeh, A.M.A. Hamdan, A.H. Nayfeh, Chaos and instability in a power system: primary resonant case, Nonlinear Dyn. 1 (1990) 313–339.
[17] E.H. Abed, P.P. Varalya, Nonlinear oscillations in power systems, Int. J. Electr. Power Energy Syst. 6 (1) (1984) 37–43.
[18] M.M. Liwschitz, Positive and negative damping in synchronous machines, AIEE Trans. 60 (1941) 210–213.
[19] J. Guckenheimer, P. Holmes, Nonlinear Oscillations, Dynamical Systems, and Bifurcations Vector Fields, Springer-Verlag, New York, 1983.
[20] H.E. Nusse, J.A. Yorke, Dynamics: Numerical Explorations, Springer-Verlag, NewYork, 1997.
[21] A. Wolf, J.B. Swift, H.L. Swinney, J.A. Vastano, Determining Lyapunov exponents from a time series, Phys. D 16 (1985) 285–317.